Chemical Science

Electronic Supplementary Information

Interaction anisotropy and shear instability of aspirin polymorphs established by nanoindentation

Sunil Varughese,[a] M. S. R. N. Kiran,[b] Katarzyna A. Solanko,[c] Andrew D. Bond,[c]* U. Ramamurty[b]* and Gautam R. Desiraju[a]*

[a] *Solid State and Structural Chemistry Unit, Indian Institute of Science, Bangalore 560 012, India. E-mail: desiraju@sscu.iisc.ernet.in*

[b] *Department of Materials Engineering, Indian Institute of Science, Bangalore 560 012, India. E-mail: ramu@materials.iisc.ernet.in*

[c] *Department of Physics and Chemistry, University of Southern Denmark, 5230 Odense, Denmark. E-mail: adb@chem.sdu.dk*

Experimental Details

Sample preparation

Single crystals of aspirin form **I** were obtained by slow evaporation of an ethanol solution over a period of one week. Preparation of form **II**: 5 g of aspirin were dissolved in 10 ml of acetic anhydride. The solution was stirred under reflux at 80°C for 4 hours. After heating, acetic anhydride was evaporated by slow evaporation at room temperature and the product was recrystallized from acetone/EtOH to give single crystals of **II**. All single crystals examined from the batch by single-crystal X-ray diffraction were found to be form **II**, without any measurable form **I** Bragg peaks or diffuse scattering, and the bulk sample assessed by powder X-ray diffraction showed strong diagnostic peaks for form **II**.

Powder X-ray diffraction

X-ray powder diffraction data were collected at the Indian Institute of Science on a Philips X'pert Pro X-ray powder diffractometer equipped with an X'cellerator detector, or on a Panalytical X'pert Pro diffractometer equipped with a PIXcel detector (Odense). The scan range, step size, and time per step were $2\theta = 5.00$ to 30°, 0.02^o, and 25 s, respectively.

Single-crystal X-ray diffraction

Single crystals were analysed using either a Bruker Nonius X8-APEXII instrument (Odense) or a Rigaku Mercury375R/M CCD (XtaLAB mini) diffractometer (Bangalore), both using graphite-monochromated MoKα radiation. Simulated precession images in the $h1l$ and $h\Box l$ reciprocal lattice planes were used to assess the presence of form **I** or form **II** Bragg peaks, plus any diffuse scattering along a^*. Full data sets for form **II** at 298 K (for comparison with PXRD data collected at room temperature) and at 123 K (for comparison with the form **I** structure published previously at that temperature [Bond, Boese & Desiraju, *Angew. Chem. Int. Ed.* **46**,

618–622 (2007), CSD: ACSALA14)] have been deposited with this paper.

Table S1: Crystallographic data for form **II** at 123 and 298 K

	123 K	**298 K**
CCDC No.	CCDC820967	CCDC820698
Crystal system	monoclinic	monoclinic
Space group	$P2_1/c$	$P2_1/c$
a (Å)	12.1016(4)	12.3578(7)
b (Å)	6.4721(2)	6.5315(8)
c (Å)	11.3344(4)	11.4964(7)
α (°)	90	90
β (°)	111.593(1)	112.436(3)
γ (°)	90	90
Volume (Å^3)	825.44(5)	857.69(13)
Z	4	4
Refl. measured, unique, R(int)	12065, 1552, 0.029	15790, 1527, 0.039
Refl. observed ($I > 2\sigma(I)$)	1445	1083
$R1$ ($I > 2\sigma(I)$)	0.047	0.036
$wR2$ (all data)	0.095	0.095
GOF on F^2	1.23	1.07

Calculation of intermolecular interaction energies using the SCDS-PIXEL method

All energies refer to interactions between complete molecules, quoted in kJ mol^{-1}. The numerical accuracy of PIXEL at the applied condensation factor $n = 4$ is expected to be 1–2 kJ mol^{-1}. The calculations are based on the following structures:

Form **I** at 298 K: CSD: ACSALA01 (Kim *et al.*).

Form **I** at 123 K: CSD: ACSALA14 (Bond *et al.*).

Form **II** at 298 and 123 K: CIFs with this submission (CCCD 820968 & 820967).

H atom positions are normalised along the X–H vectors in the X-ray structures to give C–H = 1.08 and O–H = 1.00 Å. Molecules are included in the cluster for calculation if the centroid-centroid distance to the kernel molecule is less than 14 Å. Centroid–centroid distances in the tables refer to the structures after H-atom normalisation.

Calculation of attachment energies

Attachment energies for the various crystal faces were calculated within Accelrys Materials Studio 4.4 (Accelrys Inc., Cambridge, UK), using the Dreiding 2.21 force field (Mayo, S. L., Olafson, B. D & Goddard W. A. *J. Phys. Chem.* **94**, 8897–8909 (1990)).

Table S2: Attachment energies and *d*-spacings for the major crystal faces in forms **I** and **II**

	Multiplicity	E_{att} (kJ mol^{-1})	d_{hkl} (Å)	% of total facet area
Form I				
{100}	2	−19.79	11.373	55.6
{002}	2	−41.51	5.699	23.2
{011}	4	−66.54	6.698	13.1
Form II				
{100}	2	−21.01	11.300	55.6
{10□}	2	−41.88	5.651	15.5
{110}	4	−64.72	5.639	12.3

Table S3: Total interaction energies **per molecule** (calculated from **all** intermolecular interactions within the cluster)

	Source	T / K	Coulomb	Polarisation	Dispersion	Repulsion	Total
Form I	ACSALA14	123 K	−103.7	−45.9	−102.0	141.6	−109.9
	ACSALA01	298 K	−98.6	−44.0	−92.6	124.0	−111.2
Form II	CCDC820967	123 K	−103.2	−46.9	−102.1	143.8	−108.3
	CCDC820968	298 K	−98.6	−44.3	−90.9	124.3	−109.5

Table S4: Sum of interaction energies **within** layers **per H-bonded dimer** (calculated from 10 interactions listed in Tables S6–S9)

	Source	T / K	Coulomb	Polarisation	Dispersion	Repulsion	Total
Form I	ACSALA14	123	−185.9	−95.3	−161.7	258.7	−184.2
	ACSALA01	298	−178.6	−92.9	−147.7	230.0	−189.2
Form II	CCDC820967	123	−186.8	−98.7	−162.3	264.8	−183.0
	CCDC820968	298	−180.2	−94.2	−145.1	232.8	−186.7

Table S5: Sum of interaction energies **between** layers **per H-bonded dimer** (calculated from 2 interactions listed in Tables S6–S9)

	Source	T / K	Coulomb	Polarisation	Dispersion	Repulsion	Total
Form I	ACSALA14	123	−21.9	−6.7	−28.9	22.5	−35.0
	ACSALA01	298	−19.2	−5.4	−25.3	16.2	−33.7
Form II	CCDC820967	123	−18.4	−5.6	−27.6	19.0	−32.8
	CCDC820968	298	−16.0	−4.4	−23.8	12.8	−31.4

Table S6: PIXEL interaction energies (kJ mol^{-1}) for form **I** at 123 K

		Symmetry Operator	Cent-Cent (Å)	Coulomb	Pol	Disp	Rep	Total
Within layers	O–H···O dimer	1–x,–y,2–z	7.750	−138.6	−68.2	−20.7	162.6	−64.9
Between layers	C(sp^2)···O dimer (**A** in main text)	2–x,1–y,2–z	5.965	−10.6	−3.6	−21.5	14.8	−20.9
Within layer	Stacked dimer along <010>	x,–1+y,z x,1+y,z	6.552	−8.9	−3.3	−17.8	10.9	−19.1
Between layers	CH$_3$···O dimer (**B** in main text)	2–x,–y,2–z	8.073	−11.3	−3.1	−7.4	7.7	−14.0
Within layer	Stacked dimer along <010>	1–x,1–y,2–z	5.520	−1.7	−3.3	−24.0	16.3	−12.7
Within layer	Adjacent dimer along <001>	x,0.5–y,0.5+z x,0.5–y,–0.5+z	6.073	−4.7	−4.1	−18.6	15.1	−12.3
Within layer	Adjacent dimer along <001>	1–x,–0.5+y,2.5–z 1–x,0.5+y,2.5–z	8.595	−6.2	−3.2	−10.5	8.8	−11.0
Within layer	Adjacent dimer along <001>	x,1.5–y,–0.5+z x,1.5–y,0.5+z	7.086	−3.0	−1.3	−11.6	5.1	−10.9

Table S7: PIXEL interaction energies for form **I** at 298 K

		Symmetry Operator	Cent-Cent (Å)	Coulomb	Pol	Disp	Rep	Total
Within layers	O–H···O dimer	–x,2–y,–z	7.783	−138.7	−69.5	−19.8	155.7	−72.3
Between layers	C(sp^2)···O dimer (**A** in main text)	1–x,1–y,–z	6.066	−9.0	−2.9	−18.9	10.6	−20.2
Within layer	Stacked dimer along <010>	x,–1+y,z x,1+y,z	6.591	−8.1	−2.9	−15.8	7.9	−18.9
Between layers	CH$_3$···O dimer (**B** in main text)	1–x,2–y,–z	8.133	−10.2	−2.5	−6.4	5.6	−13.5
Within layer	Adjacent dimer along <001>	x,1.5–y,–0.5+z x,1.5–y,0.5+z	6.117	−3.7	−3.7	−17.3	12.5	−12.2
Within layer	Stacked dimer along <010>	–x,1–y,–z	5.589	0.1	−2.6	−21.9	12.5	−12.0
Within layer	Adjacent dimer along <001>	–x,0.5+y,0.5–z –x,–0.5+y,0.5–z	8.668	−5.6	−2.8	−9.7	7.1	−11.0
Within layer	Adjacent dimer along <001>	x,0.5–y,–0.5+z	7.177	−2.6	−1.0	−10.2	3.4	−10.3

		$x,0.5-y,0.5+z$						

Table S8: PIXEL interaction energies for form **II** at 123 K

		Symmetry Operator	Centroid-Centroid	Coulomb	Pol	Disp	Rep	Total
Within layers	O–H⋯O dimer	1–x,–y,1–z	7.740	−139.7	−71.3	−20.9	168.6	−63.3
Within layer	Stacked dimer along <010>	x,–1+y,z x,1+y,z	6.472	−9.3	−3.6	−18.6	11.9	−19.6
Between layers	C(sp^2)–H⋯O and CH$_3$⋯O	2–x,–0.5+y,1.5–z 2–x,0.5+y,1.5–z	6.726	−9.2	−2.8	−13.8	9.5	−16.4
Within layer	Adjacent dimer along <001>	x,0.5–y,0.5+z x,0.5–y,–0.5+z	6.099	−4.5	−4.2	−18.5	14.6	−12.5
Within layer	Stacked dimer along <010>	1–x,1–y,1–z	5.545	−1.1	−3.0	−23.0	15.0	−12.1
Within layer	Adjacent dimer along <001>	x,1.5–y,–0.5+z x,1.5–y,0.5+z	7.065	−3.1	−1.4	−12.0	5.6	−11.0
Within layer	Adjacent dimer along <001>	1–x,–0.5+y,0.5–z 1–x,0.5+y,0.5–z	8.595	−6.1	−3.0	−10.1	8.5	−10.7

Table S9: PIXEL interaction energies for form **II** at 298 K

		Symmetry Operator	Centroid-Centroid	Coulomb	Pol	Disp	Rep	Total
Within layers	O–H⋯O dimer	1–x,–y,1–z	7.774	−141.8	−71.3	−20.0	161.1	−72.0
Within layer	Stacked dimer along <010>	x,–1+y,z x,1+y,z	6.532	−7.6	−2.7	−15.9	8.0	−18.2
Between layers	C(sp^2)–H⋯O and CH$_3$⋯O	2–x,–0.5+y,1.5–z 2–x,0.5+y,1.5–z	6.829	−8.0	−2.2	−11.9	6.4	−15.7
Within layer	Stacked dimer along <010>	1–x,1–y,1–z	5.602	0.2	−2.5	−20.5	10.5	−12.4
Within layer	Adjacent dimer along <001>	x,0.5–y,0.5+z x,0.5–y,–0.5+z	6.164	−3.7	−3.6	−16.8	11.9	−12.2
Within layer	Adjacent dimer along <001>	1–x,–0.5+y,0.5–z 1–x,0.5+y,0.5–z	8.640	−5.7	−2.8	−9.3	7.0	−10.8
Within layer	Adjacent dimer along <001>	x,1.5–y,–0.5+z	7.182	−2.3	−1.1	−10.3	3.7	−9.9

		$x,1.5-y,0.5+z$						

Thermal expansion measurements

Lattice constants were measured from single crystals of **I** and **II** at temperatures 100, 150, 200, 250 and 300 K. Data were measured for three perpendicular sections of reciprocal space using ω scans of 45° total width, frame width 0.5°. The lattice constraints were constrained in each case to monoclinic symmetry and refined by least-squares against *ca* 500 reflections in the approximate range $3.5 < \theta < 21.5°$. The expansion is referred to the same Cartesian axis system as in the main text: $e_3 \parallel c, e_2 \parallel b, e_1 \parallel (e_2 \times e_3)$.

The comparison of the thermal expansion assessed by this method is qualitatively reliable, but should not be expected to provide precise values for the coefficients of thermal expansion, on account of the limited number of data points. Coefficients of thermal expansion in the measured range 100–300 K can be obtained by a polynomial fit to the fractional strain as a function of ΔT. The closest fit to the values reported by Bauer *et al.* for form **I** (ref. 35 in the main manuscript) was obtained using a **linear** fit, and the values quoted for form **II** are therefore also derived from a linear fit.

Table S10: Coefficients of linear thermal expansion ($\alpha_{ij} \times 10^{-6}$ K^{-1}) obtained by a linear fit to the crystallographic data

ij	Form I (Bauer *et al.*)	Form I	Form II
11	92.6	81.0	65.4
22	36.8	32.4	53.6
33	80.4	58.4	73.6

Table S11: Lattice constants determined for form **I** as a function of temperature

		e_2	e_3				e_1	
T / K	$a / Å$	$b / Å$	$c / Å$	$\alpha / °$	$\beta / °$	$\gamma / °$	$d(100) / Å$	$V / Å^3$
100	11.2455(12)	6.5399(7)	11.2487(12)	90	95.897(4)	90	11.186	822.9(2)
150	11.2838(13)	6.5487(7)	11.2725(12)	90	95.812(4)	90	11.226	828.7(3)
200	11.3276(14)	6.5604(8)	11.3069(14)	90	95.741(4)	90	11.271	836.1(3)
250	11.3769(15)	6.5708(9)	11.3462(15)	90	95.723(5)	90	11.320	844.0(3)
300	11.4287(17)	6.5837(10)	11.3869(17)	90	95.672(5)	90	11.373	852.8(4)

Table S12: Strain (%) relative to the structure of form **I** at 300 K

T / K	e_1	e_2	e_3
100	−1.64	−0.67	−1.21
150	−1.29	−0.53	−1.00
200	−0.90	−0.35	−0.70
250	−0.46	−0.20	−0.36
300	0	0	0

[Data are plotted in Fig. 4 of the main manuscript]

The results are essentially identical to those derived using dilatometry by Bauer *et al.* [*Cryst. Growth. Des.* **10**, 3132–3140 (2010)].

Table S13: Lattice constants determined for form **II** as a function of temperature

T / K	a / Å	e_2 b / Å	e_3 c / Å	α / °	β / °	γ / °	e_1 $d(100)$ / Å	V / Å^3
100	12.0859(12)	6.4681(6)	11.3145(10)	90	111.528(3)	90	11.243	822.8(2)
150	12.1315(13)	6.4853(7)	11.3528(11)	90	111.621(4)	90	11.278	830.4(2)
200	12.1701(14)	6.5024(7)	11.391(12)	90	111.679(4)	90	11.309	837.7(3)
250	12.2226(16)	6.5220(8)	11.4399(13)	90	111.773(4)	90	11.351	846.9(3)
300	12.2876(18)	6.5362(9)	11.4850(15)	90	111.965(5)	90	11.396	855.5(3)

Table S14: Strain (%) relative to the structure of form **II** at 300 K

T / K	e_1	e_2	e_3
100	−1.34	−1.04	−1.48
150	−1.03	−0.78	−1.15
200	−0.76	−0.52	−0.82
250	−0.40	−0.22	−0.39
300	0	0	0

[Data are plotted in Fig. 4 of the main manuscript]

Transformation of form II → form I during mechanical grinding

Grinding experiments were carried out with a Retsch MM400 ball mill, using 25 ml stainless

steel containers with one stainless steel ball (Ø 15 mm), shaken at 17.5 Hz for 30 min.
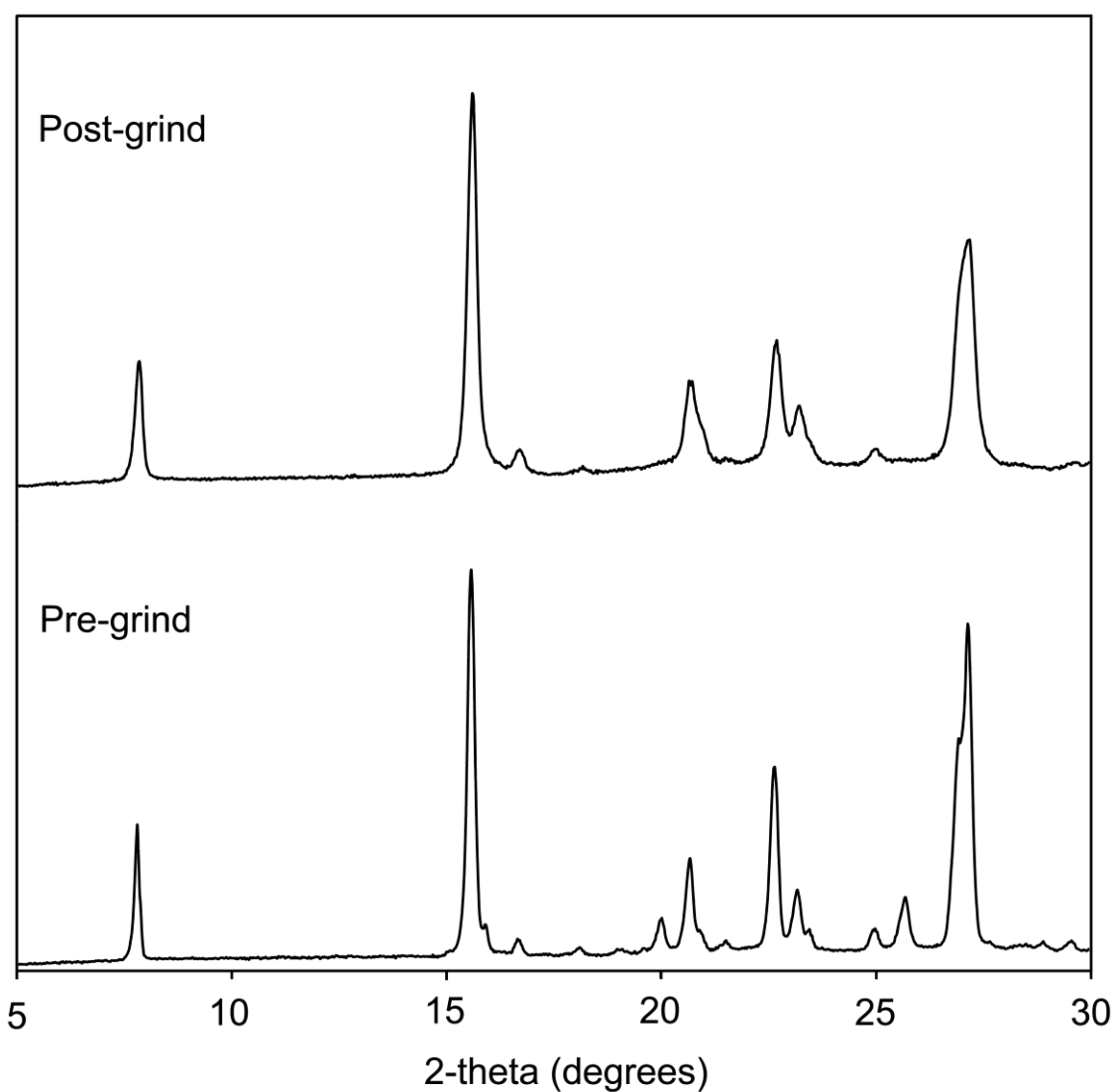
Figure S1: PXRD data for bulk samples before and after mechanical grinding. The principal

diagnostic peaks for form **II** occur at $2\theta \approx 19.9$ and $25.5°$.

Nanoindentation: practical details

Crystals of approximate dimensions $1.5 \times 0.5 \times 0.15$ mm were firmly mounted on a stud using a very thin layer of cyanoacrylate glue before nanoindentation. Around six to seven crystals were used in several analyses. The analyses were performed on the {100} and {001} faces of **I** and on the {10$\square$} and {100} faces of **II** using a nanoindenter (Triboindenter of Hysitron, Minneapolis, USA) with an *in situ* imaging capability. The machine continuously monitors and records the load, *P*, and displacement, *h*, of the indenter with force and displacement resolutions of 1 nN and 0.2 nm, respectively. A three-sided pyramidal Berkovich diamond indenter with a sharp tip (end radius ~100 nm) was used to indent the crystals. The loading and unloading rates of 0.6 mN/s and a hold time of 30 s at peak load were employed. In order to identify flat regions for the experiment, the crystal surfaces were imaged prior to indentation using the same indenter tip. A minimum of 30 indentations were performed on each crystallographic face. The indentation impressions were captured immediately after unloading so as to avoid any time-dependent elastic recovery of the residual impression. The *P-h* curves were analyzed using the standard Oliver-Pharr (O-P) method to extract the elastic modulus, *E*, of the crystal in that orientation [Oliver, W. C. & Pharr, G. M., *J. Mater. Res.* **7**, 1564–1583 (1992)]. However, this method was not employed for estimation of the hardness, *H*, on {100} of **I** since there was significant plastic flow during indentation, which resulted in pile-up of material against the indenter. Such pile-up, when present, makes the estimation of *H* using the O-P method inaccurate. Therefore, *H* was determined from the maximum indentation load, P_{max}, divided by the contact area, *A*, the latter being estimated from images of the indentation impressions.

Nanoindentation: methodology

The nanoindentation analyses were conducted using quasi-static (load-controlled) mode. Contact stiffness, S, is determined from the slope of the load-displacement (P-h) curve at the initial point of unload (*i.e.* $S = dP/dh$). Therefore, **elastic modulus, E, and hardness, H, refer to that at the maximum indentation depth**. The elastic contact stiffness determined from the P-h curves is used to calculate the reduced modulus, E_r, according to the following equation:

$$E_r = \frac{\sqrt{\pi}}{2\beta} \frac{S}{\sqrt{A_c}}$$

where A_c is the contact area under load (based on the calibrated tip areal function) and β is a constant that depends on the geometry of the indenter ($\beta = 1.034$ for a Berkovich tip). The Oliver-Pharr method to extract the sample elastic modulus from the reduced modulus assumes isotropic elastic properties, which is normally not the case for single crystals. To account for the effects of anisotropy in single crystals, the modulus obtained from nanoindentation of a single crystal is more appropriately represented as an ''indentation modulus'', given by:

$$\frac{1}{E} = \frac{1-v_i^2}{E_i} + \frac{1-v_s^2}{E_s}$$

where v and E are Poisson's ratio and elastic modulus, respectively; and the subscripts i and s refer to the indenter and test material, respectively. The indenter properties used in this study are $E_i = 1141$ GPa, and Poisson's ratio for the indenter is $v_i = 0.07$. The hardness of a material is defined as its resistance to local plastic deformation. Thus, indentation hardness, H, can be determined from the maximum indentation load, P_{max}, divided by the contact area, A:

$$H = \frac{P_{max}}{A}$$

where A is a function of the contact depth, h_c, and can be determined by the following equation:

$$A(h_c) = C_0 h_c^2 + C_1 h_c + C_2 h_c^{1/2} + C_3 h_c^{1/4} + ... + C_8 h_c^{1/128}$$

If it is assumed that a Berkovich indenter has a perfect tip, only the constant C_0 need be used. For imperfect tips, however, the higher-order terms must be taken into account and these are obtained from the tip-area function curve fit for a given tip.
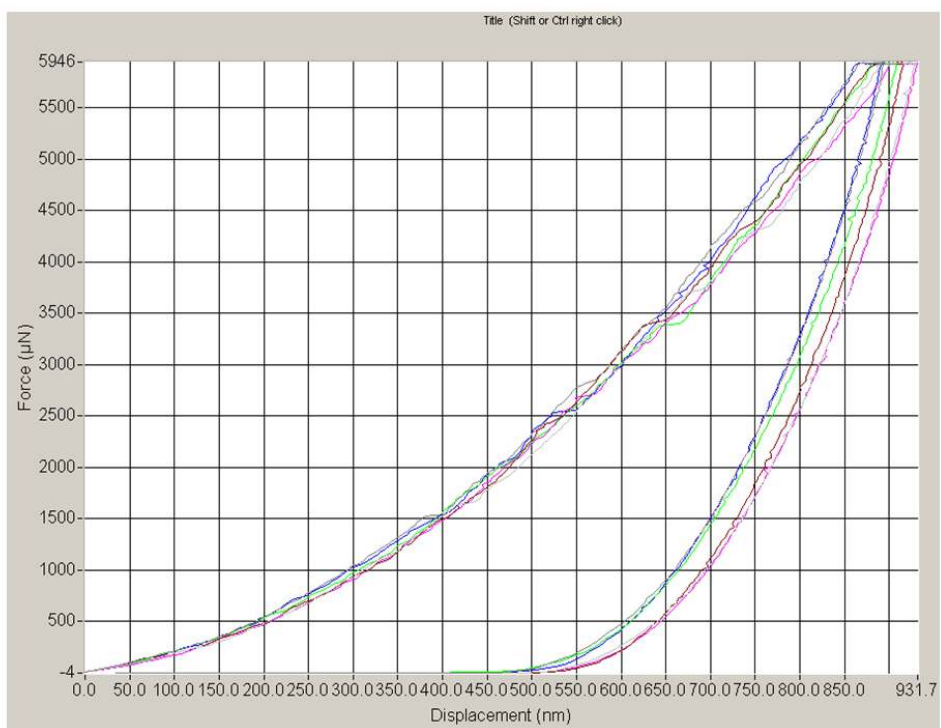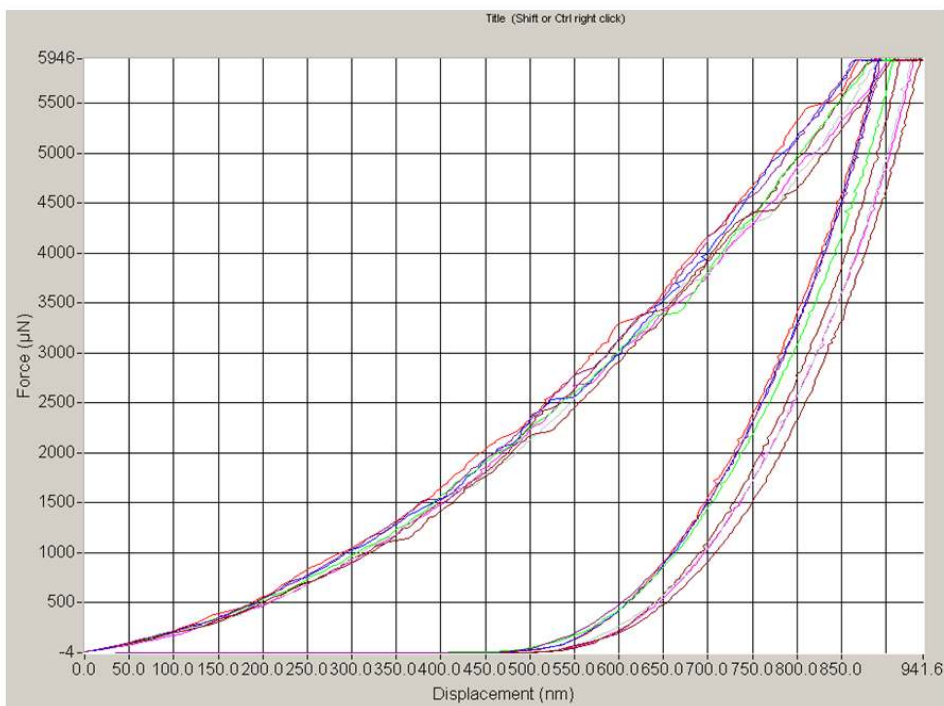
The contact depth can be estimated from the load-displacement data using:

$$h_c = h_{max} - \varepsilon \frac{P_{max}}{S}$$

where h_{max} is the maximum indentation depth and 0.75 (P/S) denotes the extent of elastic recovery (h_e).
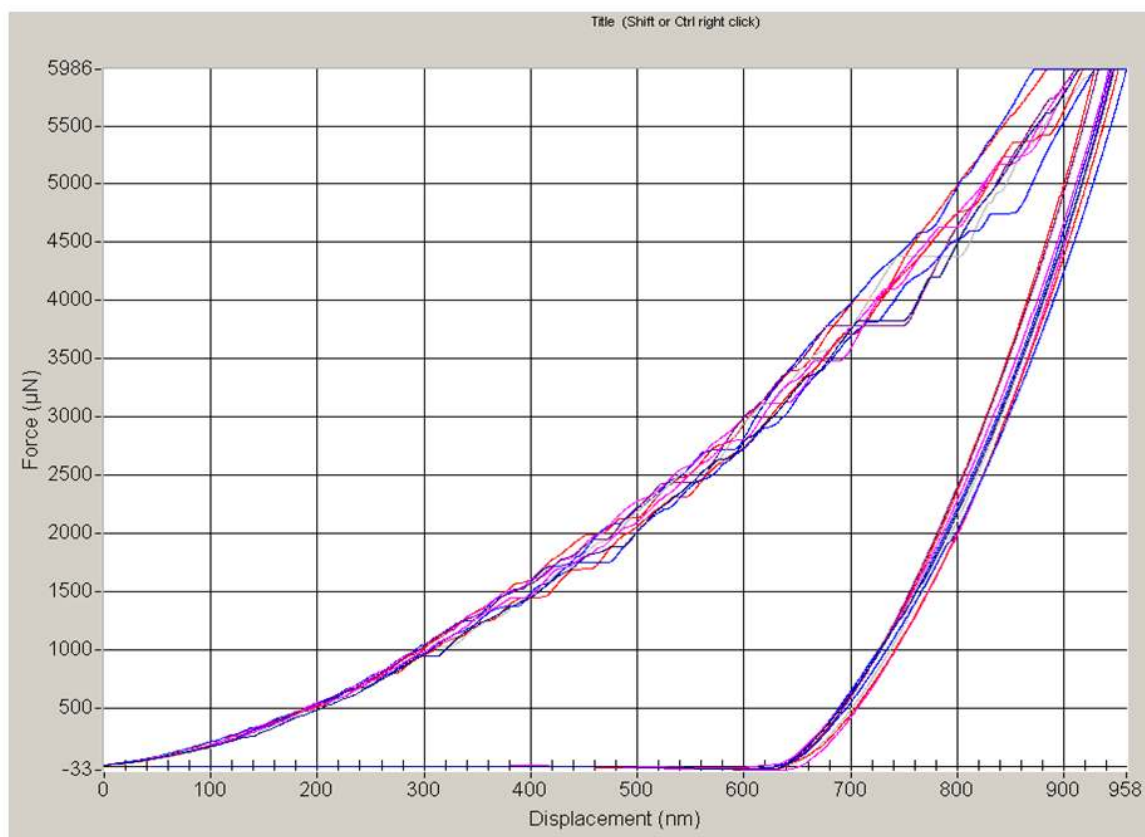
Figure S2: Load-displacement curves that show the repeatability and reliability of the indentation experiments on {100} of aspirin form **I**.
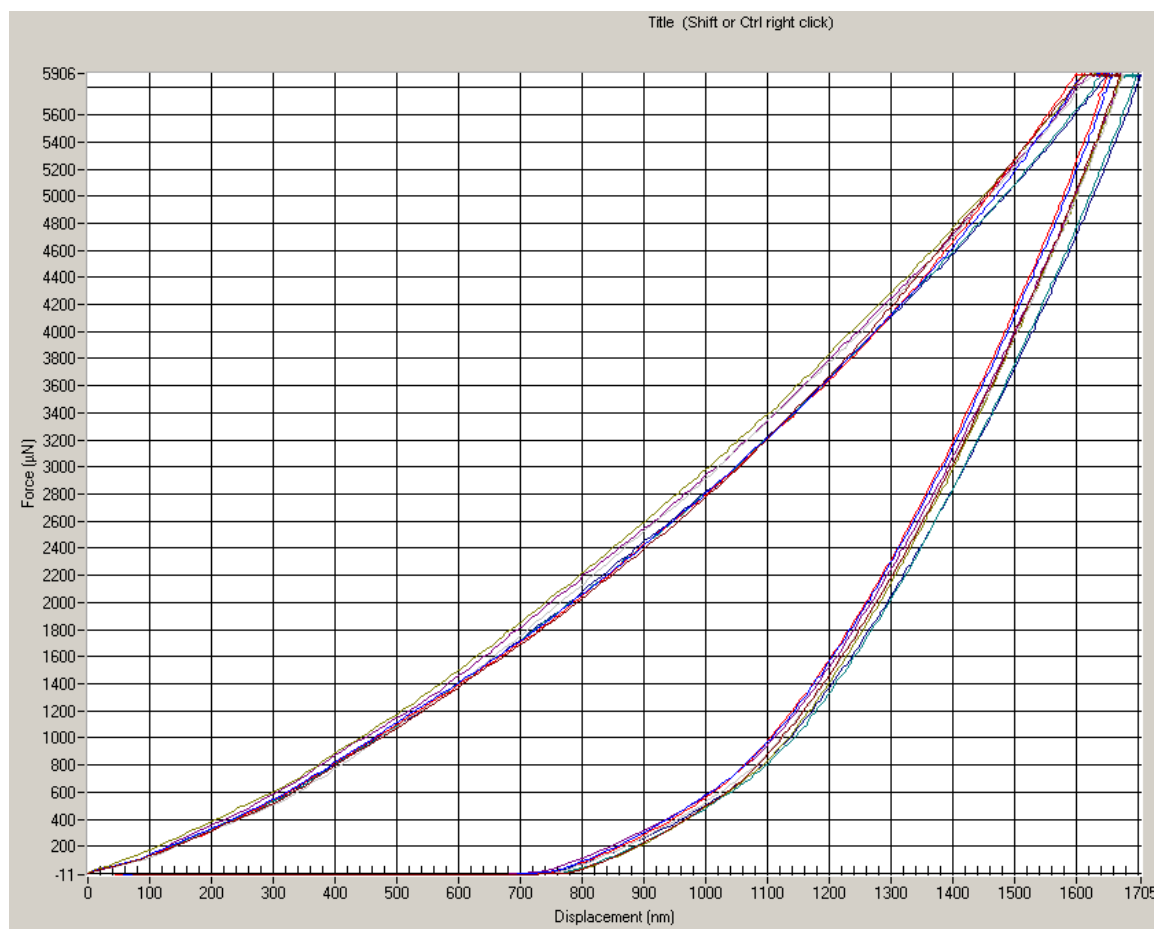
Figure S3: Load-displacement curves show the repeatability and reliability of the indentation experiments on {001} of aspirin form **I**. The two figures represent the *P-h* curves obtained from different crystals. The loading curves are not as smooth as that of {10□} of **II**: several serrations are observed, which can be attributed to strain developed in the system as discussed in the main text. These serrations may be observed as pop-ins at higher loads or

S18

loading rates. Further, {001} of the crystal is not as smooth as {100} of **I** and in fact is reflected in the higher scattering observed in the unloading curves.
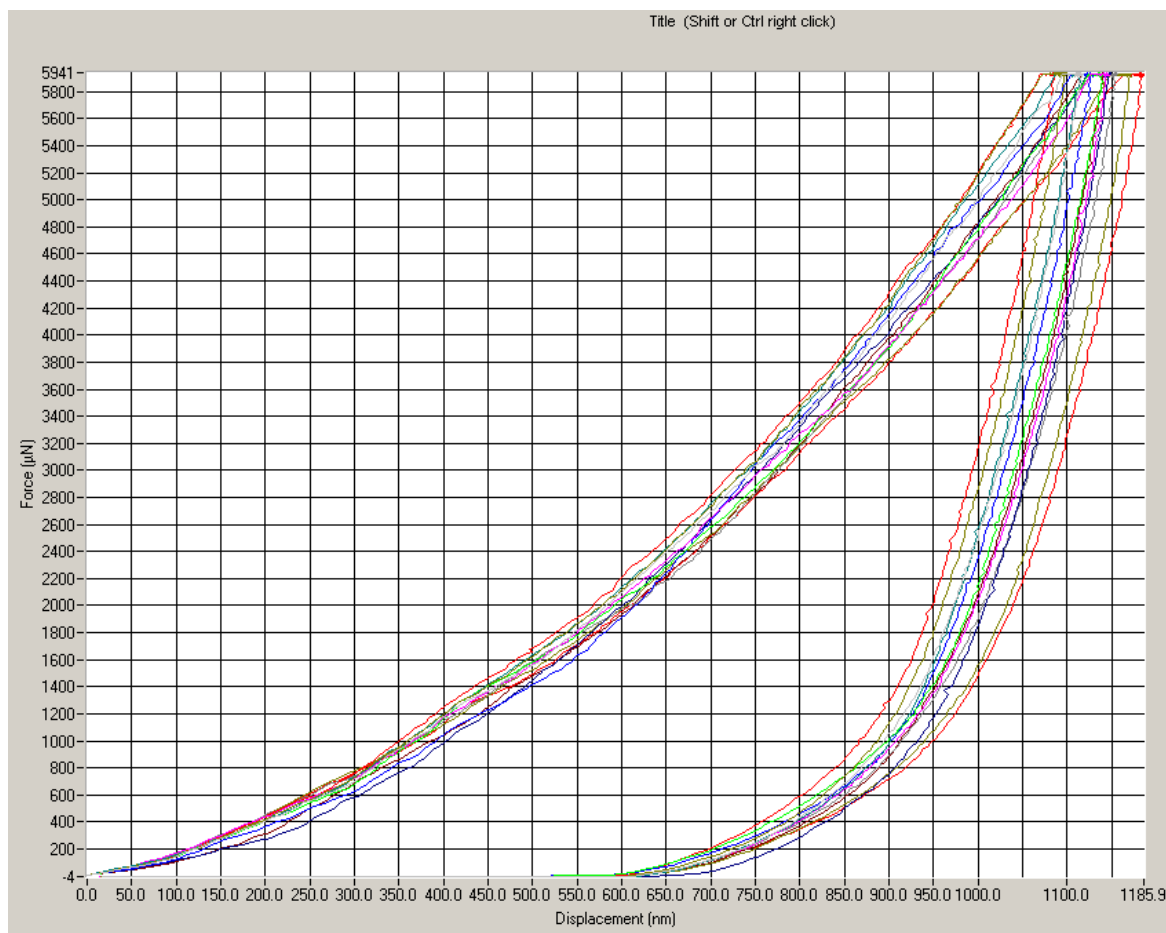

**Figure S4**: *P-h* curves corresponding to {10□} of **II**.

Figure S5: Load-displacement curves show the repeatability and reliability of the indentation experiments on {100} faces of aspirin form **II**. Note that the penetration depth is close to 1700 nm at a load of 6 mN.
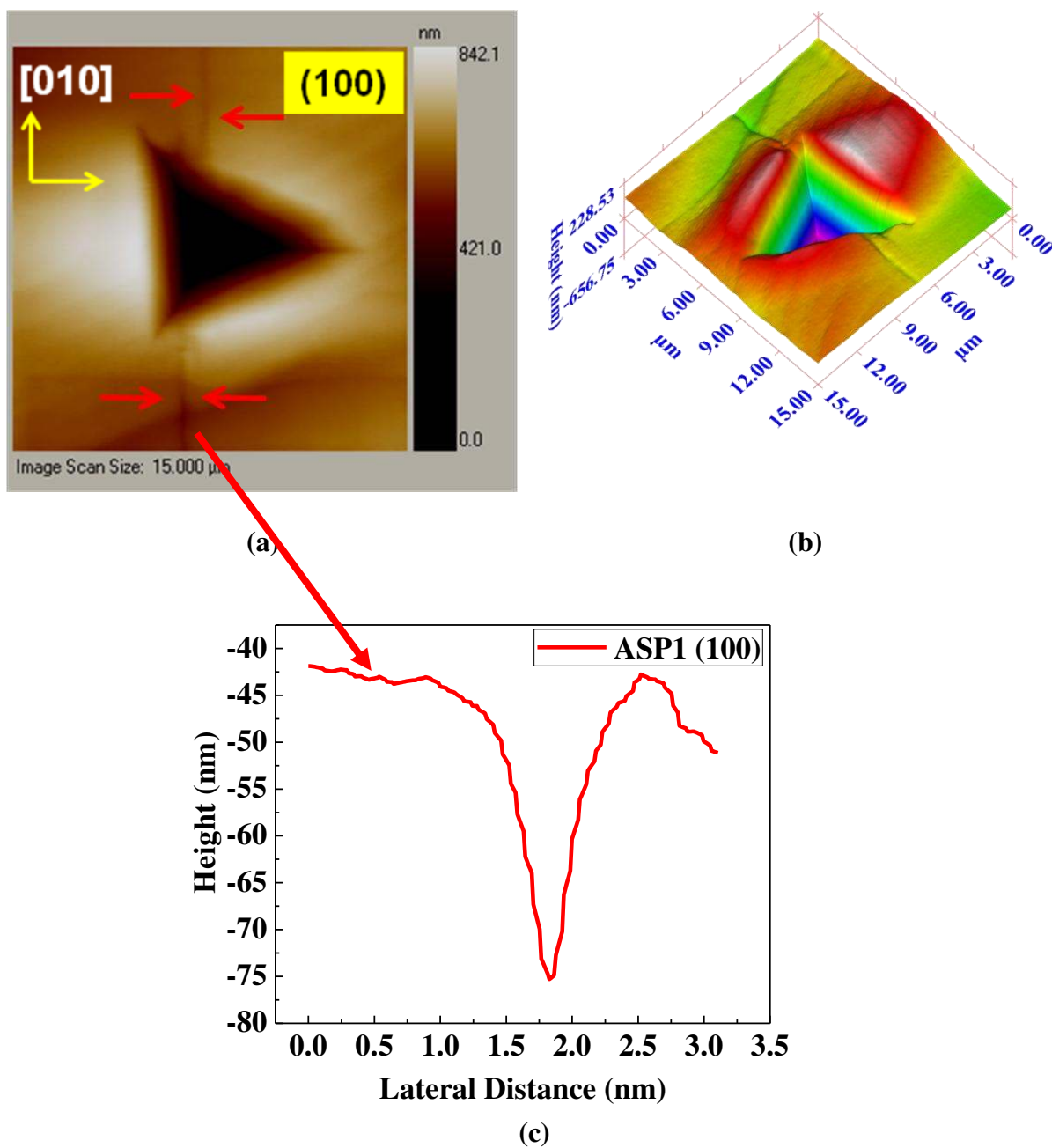
Figure S6: a, Atomic force microscope image of the residual indent impression on the {100} face of aspirin form **I** shows radial cracks along <010> when indented at a load of 6 mN, **b**, shows the corresponding 3-D image and **c** shows crack width and depth.
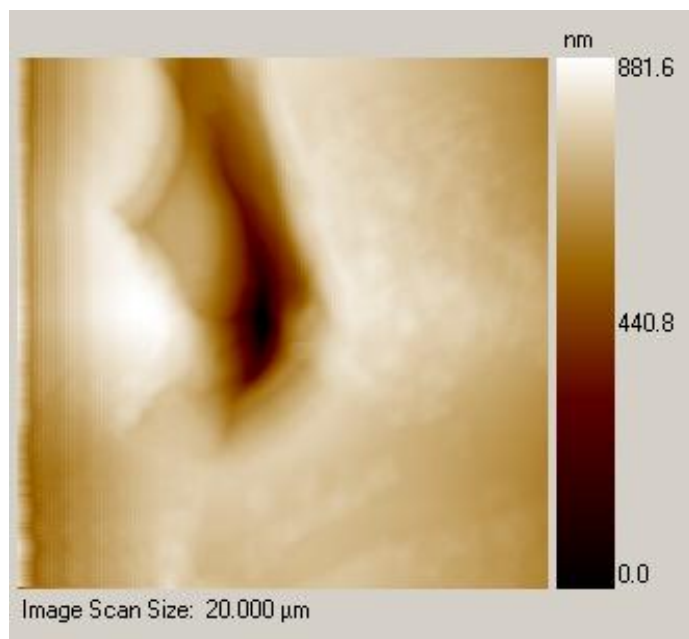
(a)
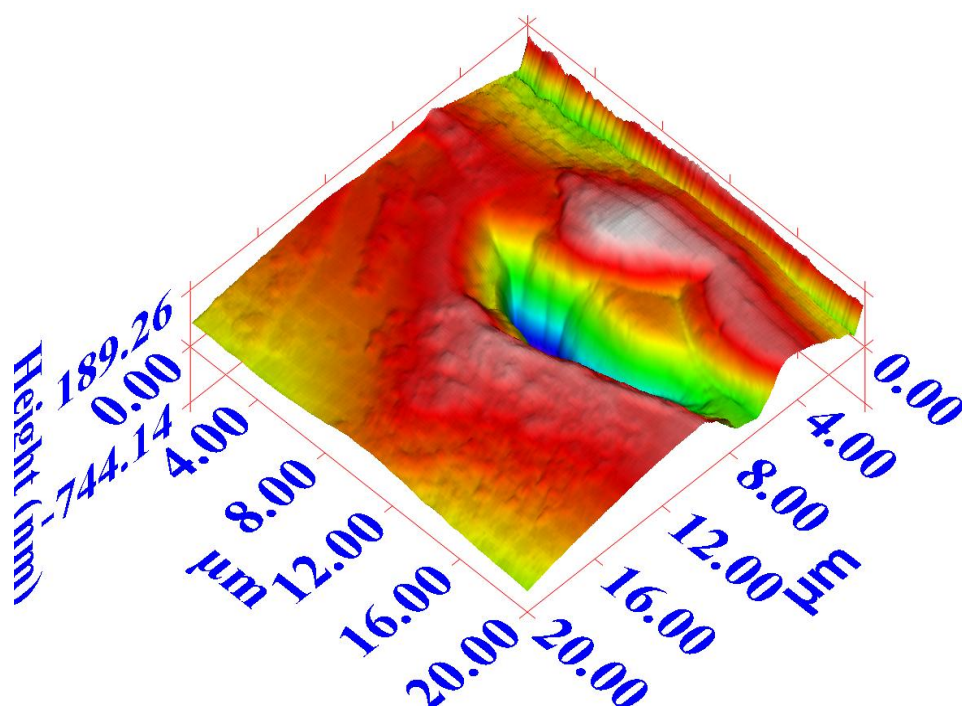
(b)

Figure S7: Residual indent impression on {100} face of aspirin form **II**. **a**, Topographic

image, **b**, 3D view.